Turkish Journal of Electrical Engineering & Computer Sciences

http://journals.tubitak.gov.tr/elektrik/

Research Article

Turk J Elec Eng & Comp Sci
(2016) 24: 2838 – 2852

doi:10.3906/elk-1404-292

Wind farm based on DFIG entirely interfaced with 14-node distribution network: power control and voltage regulation

Rabah BABOURI*, Ounissa AOUCHENNI, Djamel AOZELLAG, Kaci GHEDAMSI
Laboratory of Renewable Energy Mastery, Faculty of Technology, University of Bejaia, Bejaia, Algeria

Received: 15.04.2014 • **Accepted/Published Online:** 20.12.2014 • **Final Version:** 15.04.2016

Abstract: High penetration of wind energy into the network may introduce stability and power quality problems due to the fluctuating nature of the wind and the increasing complexity of the power system. This paper describes a novel approach to voltage and power control of a radial electrical distribution network, using a wind farm. The wind farm consists of seven 75 kW induction generators (DFIG) supplying two AC/DC converters. The feed structure of the DFIG allows operating the system conversion in a wide range of speed variations. That is why it is a recommended solution, due to its capacity to increase the generator power to twice its nominal power; consequently, the system's size and cost are reduced. Another advantage is that the system is decoupled with an electrical network, so the disturbances do not affect the DFIG and this also avoids the problems of coupling the machine to the power grid. Through a 14-node distribution network, this study proves that the method is feasible. A simulation work was carried out with the software MATLAB/Simulink. The results obtained prove that this control is suitable for regulating the desired power flows in a power network and providing the best voltage profile in the system, as well as minimizing the system transmission losses when inserting the wind farm into the electrical network.

Key words: DFIG, voltage regulation, radial distribution network, wind generation, power control

1. Introduction

The main problem regarding wind power systems is the major discrepancy between the irregular character of the primary source (wind speed is a random, strongly nonstationary process, with turbulence and extreme variations) and the requirements imposed regarding the electrical energy quality: reactive power, harmonics, flicker, etc. Thus, wind energy conversion within the parameters imposed by the energy market and by technical standards is not possible without the essential contribution of automatic control [1–4]. Due to the intermittence and fluctuating nature of the wind, the power quality and stability of the network can be affected when high wind power integration is performed. Therefore, a high penetration rate of wind energy into the power grid, which was built based on large synchronous generators, may lead to a convenient redesign [5–7]. In recent years DFIG is increasingly used in wind energy conversion systems (WECSs), due to its ability to operate at maximum power point tracking (MPPT), over a wide range of speed variations, and with increasing energy capture capacity. Most works on this machine have studied the structure where the stator is directly connected to the network and the rotor is powered by a power electronics converter, as in [8–12], and the advantage of this solution is that the converter is sized at 30% of the rated power of the system and therefore the speed variation limit is near the synchronization speed [13–18]. However, the objective of this work is radial electrical

*Correspondence: rabah.babouri@yahoo.fr

distribution network voltage control, using a wind frame based on DFIG operating over a wide range of speed variation. The stator and the rotor of each generator are connected to the common DC link bus through two rectifiers, as shown in Figure 1, so the grid inverter side is sized to the total wind farm power.

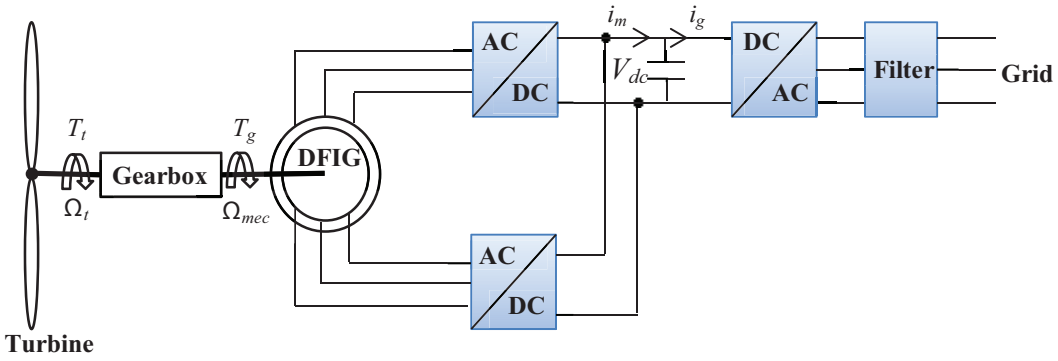

Figure 1. DFIG entirely interfaced with network.

Electrical distribution networks were not designed to deal with significant power injections from WECSs, and therefore the anticipated proliferation of a WECS results in a number of network planning and operational challenges, including voltage control, protection issues, altered transient stability, bidirectional power flow, and increased fault levels; voltage variation has been identified as one of the dominant effects [15]. Many papers, such as [1,2,16,17], discussed the problem of WECS connection in electrical networks, regulating the desired power flows, and providing the best voltage profile [1]. As demonstrated, the inherent characteristics of a wind turbine (aero-generator) and the volatility of the wind cause variations in system voltage. Therefore, a wind turbine requires high reactive power compensation. A flexible AC transmission system (FACTS) device such as a static compensator (STATCOM) can be used to control the reactive power injected into the power grid. The integration impacts of wind power on the voltage stability and the powers forwarded into the lines of an electrical network were presented in [3], where the authors proposed to insert a FACTS device, which was a STATCOM, at the place of integration of the wind power for the voltage adjustment. Continuous expansion of the electrical distribution network along with the increased installation of the WECS at a medium voltage level leads to increasing the short-circuit current at some points of the network. In [18] the network constrained setting of voltage control variables based on probabilistic load flow techniques was presented. The method determines constraint violations for a whole planning period together with the probability of each violation and leads to the satisfaction of these constraints with a minimum number of control corrective actions in a desired order. The method is applied to define fixed positions of tap-changers and reactive compensation capacitors for voltage control of a realistic study case network with increased wind power penetration. In this paper, a novel approach to voltage control of radial electrical distribution networks with a connected wind farm is introduced (see Appendix for parameters). A reliable control strategy based on the fuzzy logic of the inverter is developed in order to ensure the system stability regarding power quality and voltage level; this inverter is exploited for the active power transit from the wind farm to the network, voltage regulation, and maintenance of it within the limits at the connection node of this farm.

2. Wind generator model

2.1. Modeling of the wind turbine and gearbox [19,20]

The aerodynamic power converted by the wind turbine is dependent on the power coefficient C_p:

$$P_t = \frac{1}{2} C_p(\lambda) \rho \pi R^2 V_w^3, \tag{1}$$

where $\rho$is the air density, R the blade length, V_w is the wind speed, and C_p is the performance coefficient, which has been approximated using the flowing function:

$$C_p = (0.44 - 0.0176\beta) \sin\left(\frac{\pi(\lambda - 1)}{15 - 0.3\beta}\right) - 0.00184(\lambda - 1). \tag{2}$$

In this work the pitch angle β is fixed to zero ($\beta = 0$) so the expression of the performance coefficient is simplified as follows:

$$C_p = 0.44 \sin\left(\frac{\pi(\lambda - 1)}{15}\right). \tag{3}$$

λ is the tip speed ratio, expressed as:

$$\lambda = \frac{RV_w}{\Omega_t}. \tag{4}$$

The turbine torque is the ratio of the output power to the shaft speed:

$$T_t = \frac{P_t}{\Omega_t}. \tag{5}$$

The turbine is normally coupled to the generator shaft through a gearbox whose gear ratio G is chosen in order to set the generator shaft speed within a desired speed range. Neglecting the transmission losses, the torque and shaft speed of the wind turbine, referred to the turbine side of the gearbox, are given by:

$$T_g = GT_{em} \text{ and } \Omega_t = \frac{\Omega_{mec}}{G}. \tag{6}$$

2.2. DFIG model and vector control [21]

The classical electrical equations of the DFIG in the PARK frame are written as follows:

$$\begin{cases} \nu_{sd} = R_s i_{sd} + s\varphi_{sd} - \omega_s \varphi_{sd} \\ \nu_{sq} = R_s i_{sq} + s\varphi_{sq} + \omega_s \varphi_{sd} \\ \nu_{rd} = R_r i_{rd} + s\varphi_{rd} - (\omega_s - \omega)\varphi_{rq} \\ \nu_{rq} = R_r i_{rq} + s\varphi_{rq} + (\omega_s - \omega)\varphi_{rd} \end{cases}, \tag{7}$$

where R_s and R_r are respectively the stator and rotor phase resistances, $\omega = p\Omega_{mec}$ is the electrical speed, $p$is the number of pair poles, and s is the Laplace operator.

A vector-controlled doubly fed induction machine is an attractive solution for highly restricted speed range electric drive and generation applications; it consists in guiding an electromagnetic flux of the DFIG along the axis d or q [21]. In our case, we choose the direction of reference (d, q) according to the direct stator flux vector φ_{sd}, so the DFIG steady-state model will be simplified as follows:

$$\begin{cases} \nu_{sd} = R_{sd} i_{sd} \\ \nu_{sq} = R_s i_{sq} + \omega_s \varphi_{sd} \\ \nu_{rd} = R_r i_{rd} - \omega_r \varphi_{rq} \\ \nu_{rq} = R_r i_{rq} + \omega_r \varphi_{rd} \end{cases}, \tag{8}$$

such that:

$$\omega = \omega_s - \omega_r \omega_r = \omega_s - \omega \tag{9}$$

These simplifications lead to the reference current expressions:

$$i_{sq-ref} = \frac{T_{em-ref}}{p\varphi_{ref}},\ i_{sq-ref} = \frac{-L_s}{M} i_{sq}\,. \tag{10}$$

The machine magnetization is assured equally by the stator and the rotor side, so:

$$i_{sd-ref} = i_{rd-ref} = \frac{\varphi_{sref}}{M + L_s}. \tag{11}$$

3. Model of the network link

The DFIG is connected to the grid through three PWM converters, a DC bus, and a filter, as shown in Figure 1.

3.1. Converters model

The matrix giving the model of power electronics converters used is expressed as follows:

$$\begin{bmatrix} v_{an} \\ v_{bn} \\ v_{cn} \end{bmatrix} = \frac{1}{3} u_{dc} \begin{bmatrix} 1 & -1 & 0 \\ 0 & 1 & -1 \\ -1 & 0 & 1 \end{bmatrix} \begin{bmatrix} S_a \\ S_b \\ S_c \end{bmatrix}. \tag{12}$$

3.2. DC bus model

The equation giving the model of the DC bus is as follows:

$$u_c = \frac{1}{C} \int i_c dt, \tag{13}$$

such that:

$$i_c = (i_m - i_g). \tag{14}$$

i_m : Sum of the currents modulated by the two machine side converters.

i_g: Current modulated by the grid-side converter.

The block diagram of the DFIG control is shown in Figure 2.

4. Compensation and voltage control

The term power quality, in relation to a wind turbine, describes the electrical performances of the wind turbine generation system. The main influences of the integration of wind turbines on power quality are voltage changes and fluctuations leading to flickers and harmonics. The flickers caused by wind fluctuations may be important in low-voltage transmission lines, unlike in the high-voltage lines, and the voltage drop related to power swing is small because of the small current fluctuation for a given wind fluctuation [1].

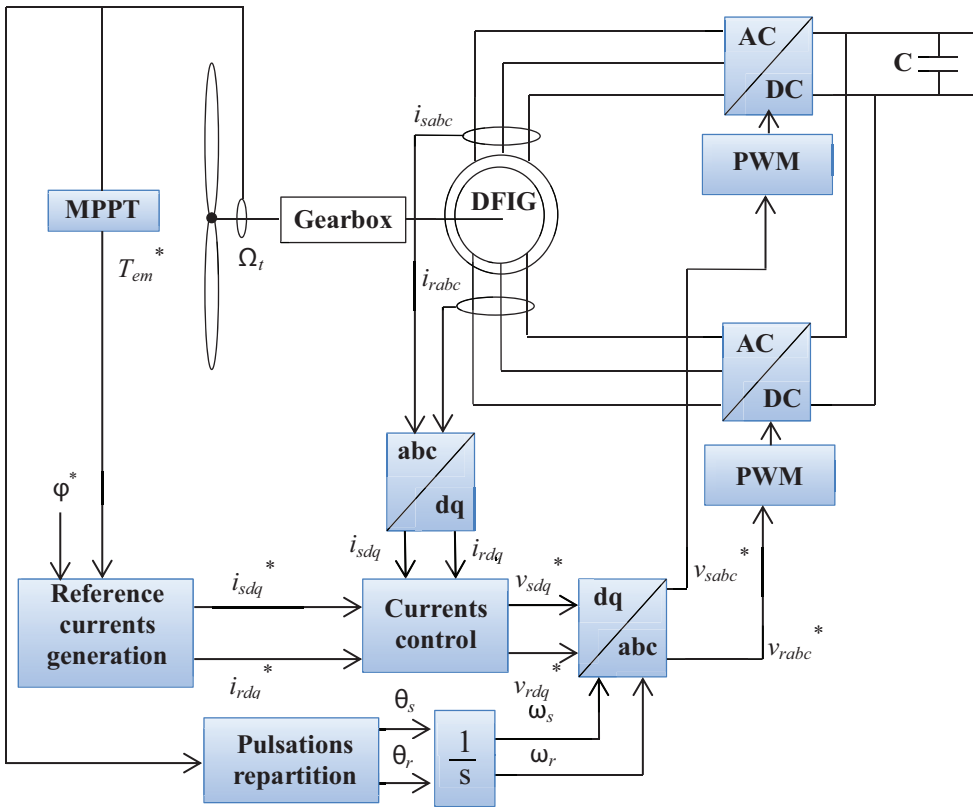

Figure 2. Control diagram of the WECS based on DFIG entirely interfaced with electrical network.

4.1. Voltage regulation

To develop a good qualitative understanding of the need for reactive power control, let us consider a simple case of a transmission line; its one-phase equivalent circuit is illustrated in Figure 3. The phasor showing the relationship between voltages and currents is given in Figure 4 [1,22,23].

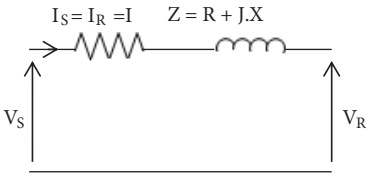

Figure 3. One-phase equivalent circuit of the power grid.

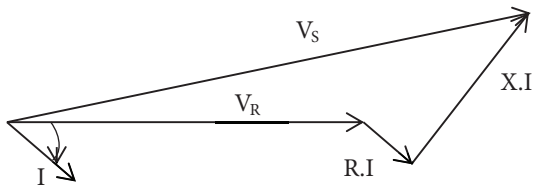

Figure 4. Phasor diagram for an inductive load.

It is clear that between the sending voltage (source voltage) and the receiving voltage (load voltage), there is a magnitude variation, and phase shift is created. Voltage regulation of the transmission line may be defined as [22]:

$$R\% = \frac{|V_S| - |V_R|}{|V_S|} \times 100 \tag{15}$$

where:

V_S : Sending end, voltage/phase;

V_R : Receiving end, voltage/phase.

The voltage drop expression in one line can be written as follows [2]:

$$\Delta V = \frac{RP + XQ}{V_R} \tag{16}$$

R : Resistance, Ω /phase;

X : Reactance, Ω/phase;

P : Active power, W;

Q : Reactive power, VAr.

For the high-voltage lines, X is widely higher than $10.R$, and Eq. (16) can be simplified as:

$$\Delta V = \frac{XQ}{V_R} \tag{17}$$

Thus, ΔV depends on reactive power flow on the line.

5. Inverter control strategy

The essential part for good performance of the controller in the inverter is the voltage detection circuit. Voltage must be detected fast and corrected. The voltage disturbance detection method is based on the error between the reference voltage magnitude V_{ref} imposed equal to 10 kV and voltage magnitude measured V_{mea} on the network. The controller system is presented in Figure 5.

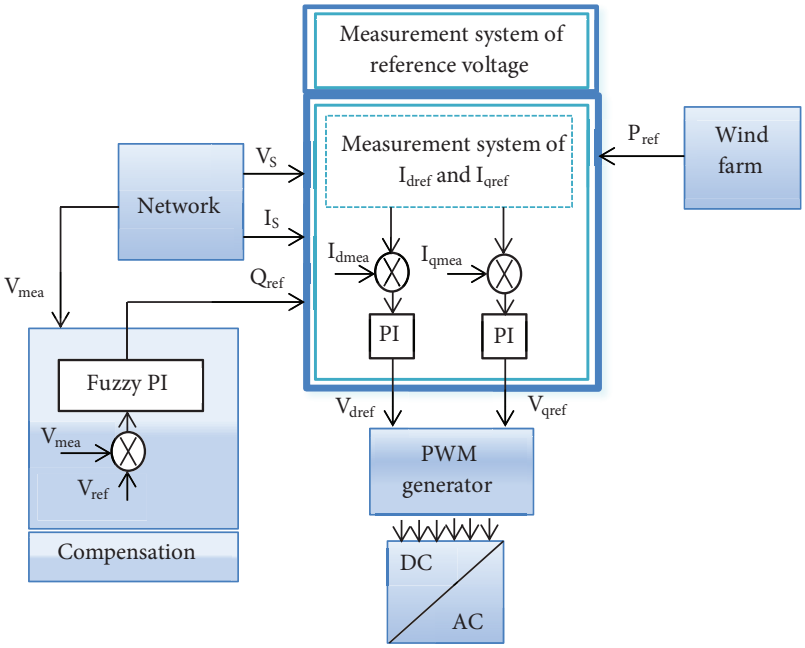

Figure 5. Control block diagram of the network side inverter control.

The three-phase supply voltage is transformed from *abc* to *odq* frame using Park transformation. A phase-locked loop (PLL) is used to track the supply voltage phase. The output of the PLL ($\Theta = \int wtdt$) is

used to compute the direct-axis and quadrature-axis components of the AC three-phase voltage and currents (labeled as V_{Sd}, V_{Sq} or I_{Sd}, I_{Sq} on the diagram represented in Figure 5 [24].

Here:

$$|V_S| = \sqrt{V_{Sd}^2 + V_{Sq}^2} \tag{18}$$

When voltage drop or overvoltage is detected, the inverter switches into active mode to react as fast as possible to inject or absorb a quantity of reactive power Q_{ref} in order to provide the best voltage profile in the system as well as to minimize the system transmission losses. Therefore, the reactive power is generated according to the difference between the reference voltage and the measured voltage and it is applied to the VSC to produce the preferred voltage profile, using the voltage control based on fuzzy controller. The reference active power P_{ref} is imposed equal to the power generated by the wind farm. The active and reactive powers forwarded are given by Eqs. (19) and (20), respectively.

$$P = V_{Sd}I_{Sd} + V_{Sq}I_{Sq} \tag{19}$$

$$Q = V_{Sq}I_{Sd} - V_{Sd}I_{Sq} \tag{20}$$

Park components of the reference currents are given by Eqs. (21) and (22).

$$I_{dref} = \frac{P_{ref}V_{Sd} + Q_{ref}V_{Sq}}{V_{Sd}^2 + V_{Sq}^2} \tag{21}$$

$$I_{qref} = \frac{P_{ref}V_{Sq} - Q_{ref}V_{Sd}}{V_{Sd}^2 + V_{Sq}^2} \tag{22}$$

Here:

$I_{dref}I_{qref}$: Park components of the reference currents;

$V_{dref}V_{qref}$: Park components of the reference voltages;

P_{ref}, Q_{ref} : Active and reactive powers references;

$V_{Sd}V_{Sq}$: Park components of V_S;

V_{mea} : Voltage measured.

The fuzzy controller used is shown in Figure 6. It is a Mamdani controller based on the max-min method, modulated with MATLAB/Simulink software. The input of the fuzzy controller is the voltage error and its variation, and the quantities concerned are noted E and dE successively, which are numerical values. The fuzzification interface transforms these numerical values into linguistic values.

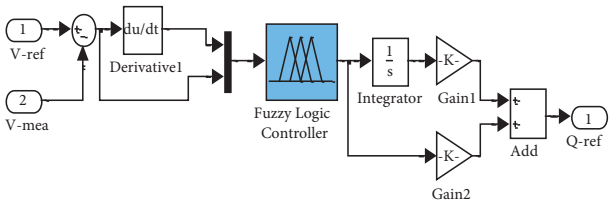

Figure 6. Voltage fuzzy controller.

Five fuzzy sets represented by membership functions (triangular and trapezoidal functions) are used for describing input and output values: large negative (LN), negative (N), zero (Z), positive (P), and large positive (LP). Figure 7 shows the five fuzzy sets of the regulator, defined graphically, such that fuzzy sets LN, Z, and LP are defined by a trapezoidal membership function and fuzzy sets N and P are defined by a triangular membership function.

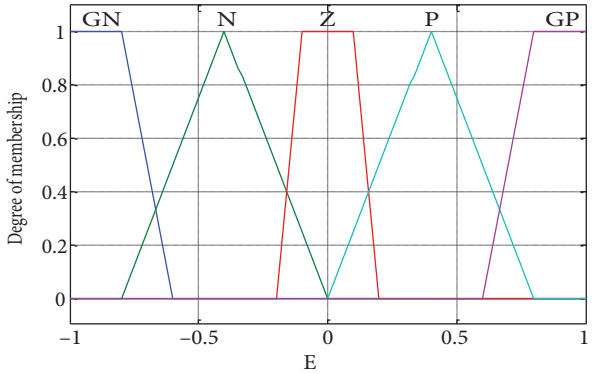

Figure 7. Graphical representation of the fuzzy sets.

A two-dimensional array is used to describe the inference engine. Entries in Table 1 represent the fuzzy sets of input variables. The intersection of a column and a line shows the fuzzy set of the output variable defined by an IF-THEN rule.

Table 1. Load data

E / dE	LN	N	Z	P	LP
LN	LN	LN	N	N	Z
N	LN	N	N	Z	P
Z	N	N	Z	P	P
P	N	Z	P	P	LP
LP	Z	P	P	LP	LP

For example, if (E is N) and (dE is LP) then (dU is P). The defuzzification interface based on the centroid method converts the linguistic values of the command to numerical values.

6. Studied system

The electrical distribution network, including the wind farm, is shown in Figure 8. The mathematic model of this system is modulated and simulated with MATLAB/Simulink software.

As can be illustrated in Figure 8, the studied electrical network is 10 kV with 14 nodes, 13 sections, 13 fixed loads, and a centralized source of power P_n equal to 4 MW. The system data are given in Tables 2 and 3. A wind farm is considered to be connected to the distribution network to bus 12.

The wind farm consists of seven 75 kW induction generators entirely interfaced with the distribution network. This wind farm will generate to the network a power P_f at an integration rate between 15% and 20%. The diagram of the wind farm is shown in Figure 9.

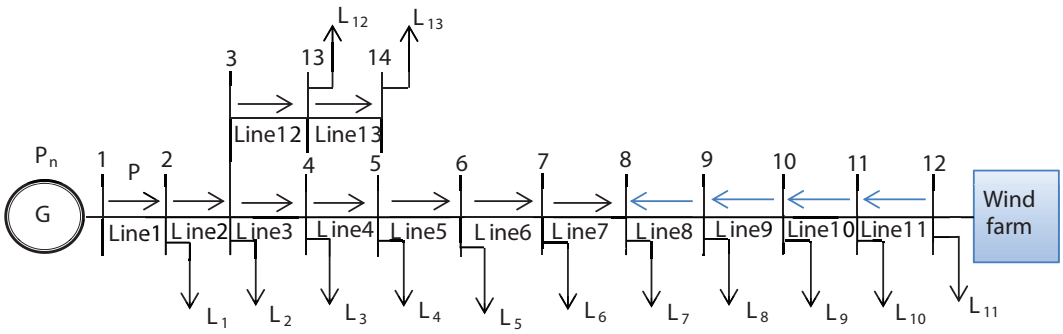

Figure 8. Electrical distribution network.

Table 2. Load data

Load	Active power (kW)	Reactive power (kVAr)
L_1	100	60
L_2	400	30
L_3	400	55
L_4	300	30
L_5	200	15
L_6	300	55
L_7	400	45
L_8	200	40
L_9	350	30
L_{10}	200	30
L_{11}	150	15
L_{12}	500	30
L_{13}	500	30

Table 3. Line data

Line	R (Ω)	X (Ω)
Line1	1.093	0.455
Line2	1.184	0.494
Line3	1.002	0.873
Line4	1.002	1.329
Line5	1.093	0.455
Line6	1.002	0.417
Line7	4.403	1.215
Line8	5.642	1.597
Line9	2.890	0.818
Line10	1.314	0.428
Line11	1.1	0.351
Line12	1.184	0.494
Line13	1.002	0.494

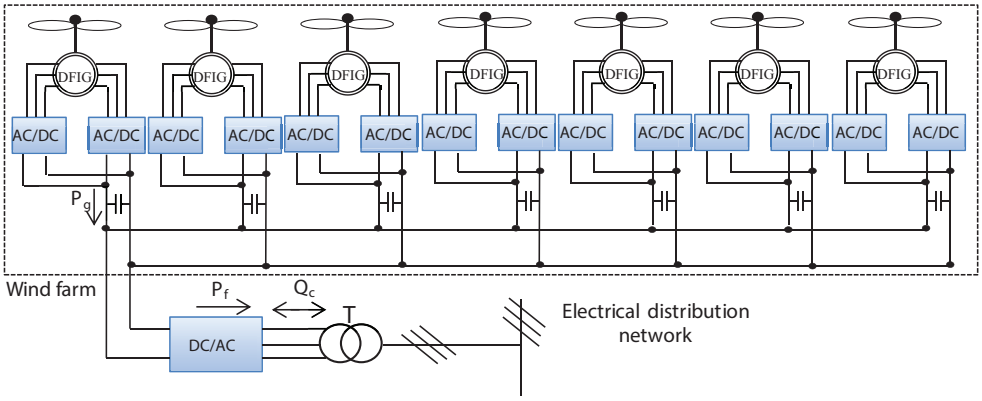

Figure 9. Diagram of the wind farm based on DFIG.

7. Simulation results and discussion

In order to study the impact of the integration of the wind farm into the electrical network, three cases of studies will be treated: a network without a wind farm; integration of the wind farm; and a network with wind farm and compensation.

7.1. Network without wind farm

In the first case, we will study only the electrical distribution network, without the wind farm and without compensation, for evaluating power losses and voltage drops in the lines. Figure 10 presents the voltage magnitudes V_B at the buses. Figures 11 and 12 show the evolution of the active P_{Lines} and reactive Q_{lines} powers injected in the lines, respectively. Figure 13 shows the evolution of the active P_{Losses} powers forwarded in lines and Figure 14 shows the voltage drops V_{Drop} in the lines. According to the simulation results, one can observe high power losses. These losses are caused mainly by resistance of conductors, where Joule losses occur, and high voltage drops in the lines can also be observed. The voltage drops are a consequence of the increased loading, increased transmission losses, and the reactive power being transported over a long distance. The highest voltage drop is recorded in bus 14 and is equal to the sum of voltage drops of all lines from the source up to this bus. The wind farm connected to the network is one of the solutions used to solve the voltage drop problem and power losses through producing power at this location of the deficit.

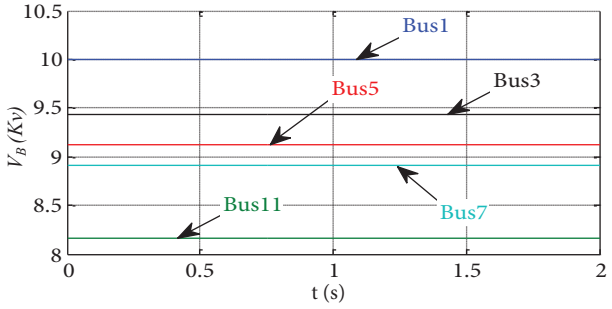

Figure 10. Voltage magnitudes at buses before integration of wind farm.

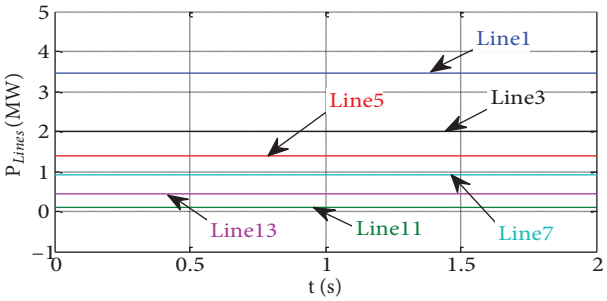

Figure 11. Active power flow on the lines.

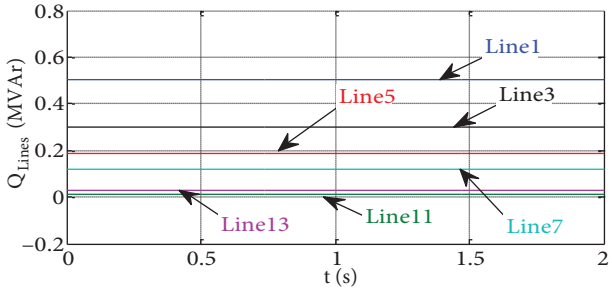

Figure 12. Reactive power flow on the lines.

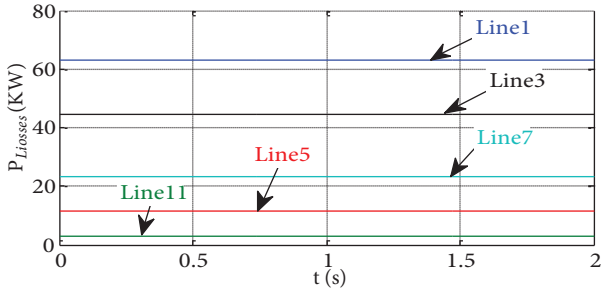

Figure 13. Active power losses flow on the lines.

7.2. Integration of the wind farm

To overcome the problem of voltage drops and power losses in the distribution network, a wind farm is connected in the bus load. Magnitudes of a single aero-generator are noted to show the advantages of the feeding structure of the DFIG. Figure 15 illustrates the DFIG speed; as we can notice, the machine operates in a wide range of speed variations, up to twice its nominal speed. The electromagnetic torque of the DFIG and the reference torque are given by Figure 16. The stator, rotor, turbine, and generator powers of the WECS are shown in Figure 17, where the power injected into the grid equals the mechanical power provided by the wind turbine, of course without taking into account the different losses. We also note that for a nominal torque and rotational speed of the machine equal to twice its rated speed, the electrical power produced by the DFIG is equal to twice

its rated power. On the other hand, the stator and rotor electric powers are almost equal, the slight difference is due to the stator resistance that is greater than the rotor resistance, and we note that the generator power is equal to the sum of the stator and rotor active powers. Figure 18 shows the regulation of the DC link voltage. Figure 19 presents the voltage magnitudes at the buses and we observe that there is an improvement of the voltage level; however, this voltage has a fluctuating form. A significant improvement of the active power losses is noted in Figure 20, showing active power losses' flow on the line. A decreasing of the voltage drops is noted in Figure 21. The active and reactive powers measured follow their references perfectly as shown in Figures 22 and 23, respectively. Figure 24 shows the evolution of the active powers forwarded in lines; it can be seen that the wind farm provides a capability to change the direction of power flow over lines 11, 10, 9, and 8 into the inverse direction.

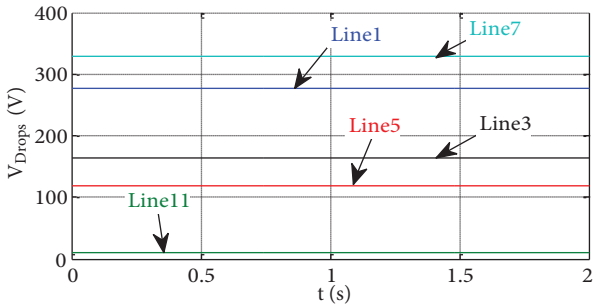

Figure 14. Voltage drops in the lines.

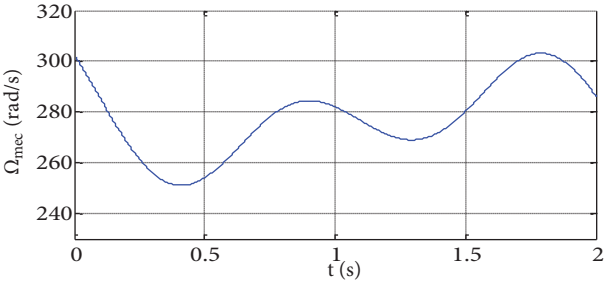

Figure 15. DFIG speed (rad/s).

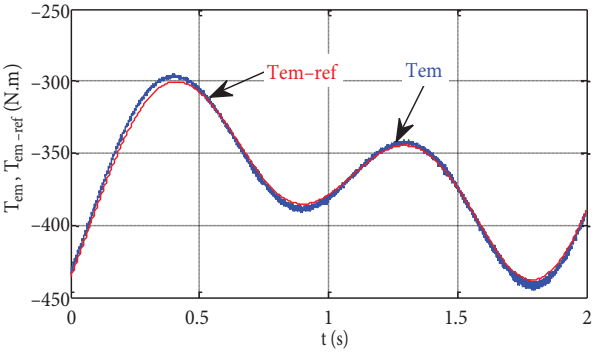

Figure 16. Electromagnetic torque and its reference.

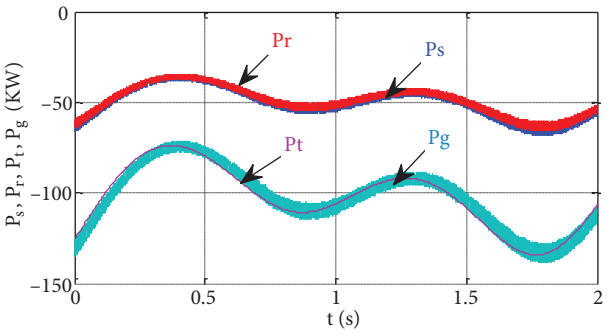

Figure 17. Stator, rotor, turbine, and grid powers.

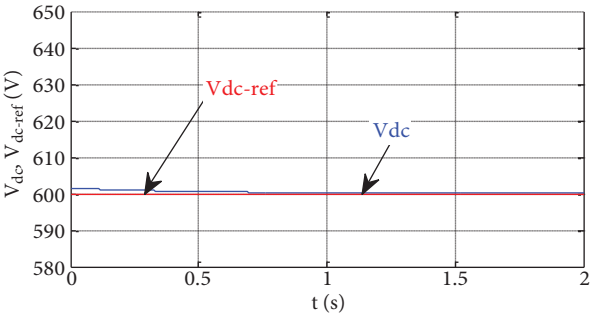

Figure 18. DC link voltage and its reference value.

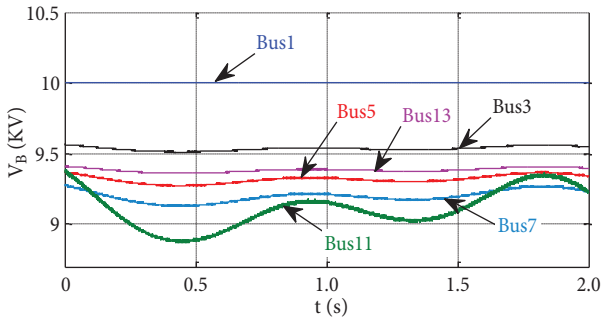

Figure 19. Voltage magnitudes at buses before compensation.

In order to solve the problem of voltage and power fluctuation caused by the power delivered by the wind farm, compensation will be made via the inverter, whose role is to provide the reactive power necessary for regulating voltage and powers flows.

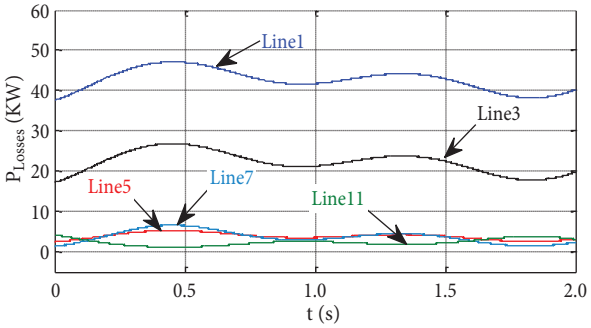

Figure 20. Active power losses in the line.

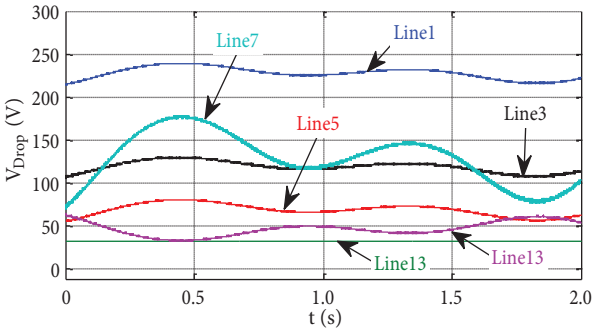

Figure 21. Voltage drops in lines.

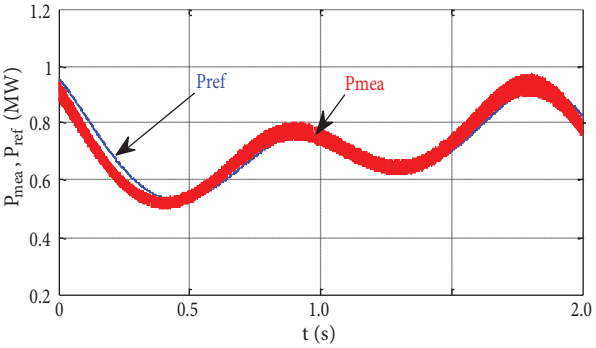

Figure 22. Measured active power and its reference.

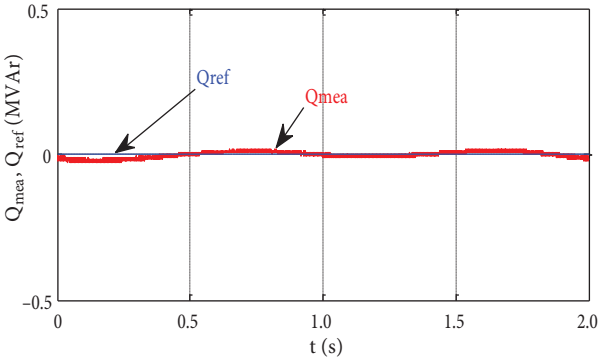

Figure 23. Measured reactive power and its reference.

7.3. Network with compensation

The results obtained show the contribution of the compensation to regulate the voltage at the connection node of the wind farm and powers transmitted through the line. Figure 25 presents the evolution of the voltage magnitudes at the buses after compensation: the voltages become very stable. Figure 26 presents the active

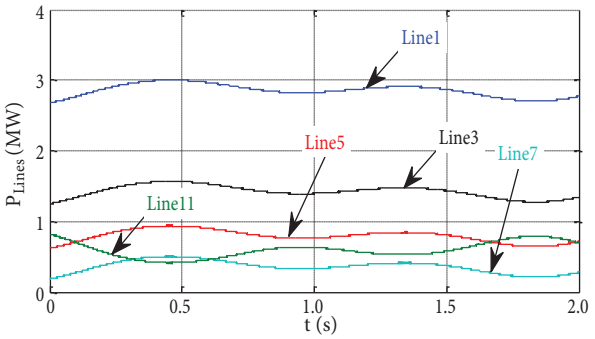

Figure 24. Active power flow on the lines.

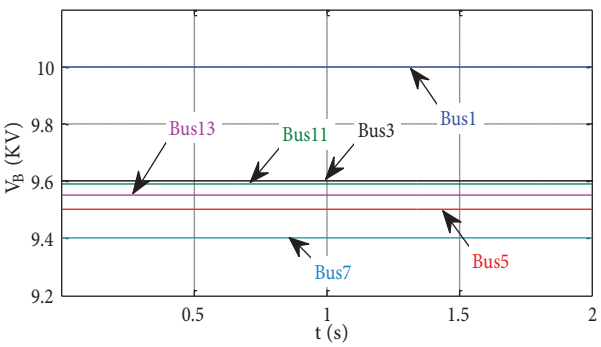

Figure 25. Voltage magnitudes at the buses after compensation.

powers provided by the source and the wind farm. Figure 27, representing the active power P_f delivered by wind farm at bus 12 and reactive compensation power Q_c, clearly shows the interest of the compensation, where the reactive power varies according to the change of active power, for maintaining a better voltage profile in the electrical distribution network.

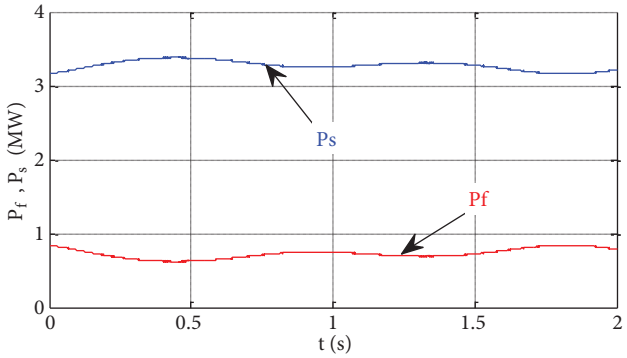

Figure 26. The source and wind farm active powers.

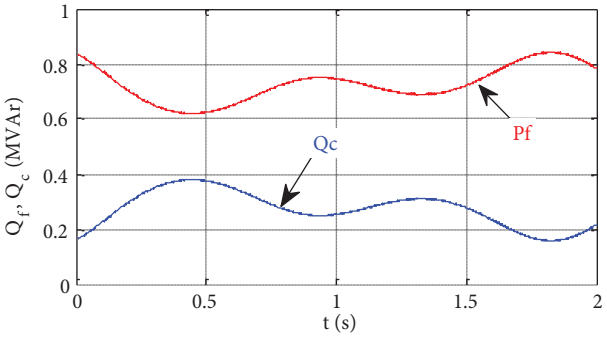

Figure 27. Active power of wind farm and reactive compensation power.

8. Conclusion

This work studied the integration of a wind farm into a 14-node distribution network, with the wind farm based on DFIG supplying two power electronic rectifiers; this topology allows us to operate the system conversion over a wide range of speed variations and improve the energy capture. The inserting of a wind farm into the network is a solution for some network problems such as power losses and voltage stability. The improvement of the voltage profile via the inverter was exploited not only for the wind farm active power transit but also to provide or to absorb reactive power in order to stabilize the voltage at the connecting node of the farm and maintain the voltage profile at the desired value. The results obtained prove the validity and reliability of the proposed study and allow the conclusion that wind energy is not only a clean and free energy but can also be used to improve network power quality.

Nomenclature

C_p	Performance coefficient
f	Viscous friction
G	Gearbox ration
i_{sd}, $i_{sq}i_{rd}i_{rq}$	Direct and quadrature stator and rotor current
i_{gd}, i_{gq}	Direct and quadrature grid current
J	Inertia
P_g	Grid power
P_r	Rotor power
P_s	Stator power
P_t	Turbine power
R	Turbine radius
T_{em}	Electromagnetic torque
T_{em-ref}	Reference torque
T_g	Generator torque
T_t	Turbine torque
u_c	DC link voltage
v_{md}, v_{mq}	Direct and quadrature voltages modulated by the inverter
v_{gd}, v_{gq}	Direct and quadrature grid voltages
v_{sd}, $v_{sq}v_{rd}v_{rq}$	Direct and quadrature stator and current voltages
V_w	Wind speed
β	Pitch angle
λ	Tip ration speed
ρ	Air density
φ_{sd}, $\varphi_{sq}\varphi_{rd}\varphi_{rq}$	Direct and quadrature stator and rotor flux
φ_{ref}	Stator reference flux
Ω_t	Turbine speed
Ω_g	Generator speed
ω_s, ω_r	Stator and rotor pulsations

References

[1] Benchagra M, Maaroufi M, Ouassaid M. A performance comparison of linear and nonlinear control of SCIG-wind farm connecting to distribution network. Turk J Electr Eng Co 2014; 22: 1-11.

[2] Aouzellag LN, Aouzellag D, Mendil B. Static compensator for maintaining voltage stability of wind farm integration to a distribution network. Renew Energ 2010; 35: 2476-2482.

[3] Aouzellag N, Aouzellag D, Mendil B. Contribution to the improvement of voltage profile in electrical network with wind generator using SVC device. Renew Energ 2010; 35: 243-248.

[4] Hajibashi M, Ebrahimi A. Markovian approach applied to reliability modeling of wind farm. Turk J Electr Eng Co 2014; 22: 287-301.

[5] Ackerman T. Wind Power in Power Systems. Chichester, UK: Wiley, 2005.

[6] Munteanu I, Bratcu A, Cutululis NA, Ceanga E. Optimal control of wind energy systems: towards a global approach. London, UK: Springer, 2008.

[7] Mathur RM, Varma RK. Thyristor-Based FACTS Controllers and Electrical Transmission Systems. New York, NY, USA: Wiley, 2002.

[8] Rahim AH, Nowicki EP. Supercapacitor energy storage system for fault ride-through of a DFIG wind generation system. Energ Convers Manage 2012; 59: 96-102.

[9] Boutoubat M, Mokrani L, Machmoum M. Control of a wind energy conversion system equipped by DFIG for active power generation and power quality improvement. Renew Energ 2013; 50: 373-386.

[10] Zaragoza J, Pou J, Arias A, Spitri C, Robles E, Ceballos S. Study and experimental verification of control turning strategies in variable speed wind energy conversion system. Renew Energ 2011; 36: 1421-1430.

[11] Heng N, Yu Q, Jiabing H. Improved control strategy of DFIG-based wind power generation systems connected to a harmonically polluted network. Electr Pow Syst Res 2012; 86: 84-97.

[12] Mohammadi J, Afsharnia S, Vaez-Zadeh S. Efficient fault-ride-through control strategy of DFIG-based wind turbines during the grid faults. Energ Convers Manage 2014; 78: 88-95.

[13] Ling Y, Cai X, Wang N. Rotor current transient analysis of DFIG-based wind turbines during symmetrical voltage faults. Energ Convers Manage 2013; 76: 910-917.

[14] Gidwani L, Tiwani H, Bansal RC. Improving power quality of wind energy conversion system with unconventional power electronic interface. Int J Elec Power 2013; 44: 445-453.

[15] Boynuegri AR, Vural B, Tascikaraoglu A, Uzunoglu M, YumurtacıR. Voltage regulation capability of a prototype static VAr compensator for wind applications. Appl Energ 2012; 93: 422-431.

[16] Roy NK, Pota HR, Hossain MJ. Reactive power management of distribution networks with wind generation for improving voltage stability. Renew Energ 2013; 58: 85-94.

[17] Girbau-Llistuella F, Sumper A, Díaz-González F, Galceran-Arellano S. Flicker mitigation by reactive power control in wind farm with doubly fed induction generators. Int J Elec Power 2014; 55: 285-296.

[18] Hatziargyriou ND, Karakatsanis TS, Lorentzou MI. Voltage control settings to increase wind power based on probabilistic load flow. Int J Elec Power 2005; 27: 656-661.

[19] Ghedamsi K, Aouzellag D, Berkouk EM. Control of wind generator associated to a flywheel energy storage system. Renew Energ 2008; 33: 2145-2156.

[20] Ghedamsi K, Aouzellag D. Improvement of the performances for wind energy conversion systems. Int J Elec Power 2010; 32: 936-945.

[21] Babouri R, Aouzellag D, Ghedamsi K. Integration of doubly fed induction generator entirely interfaced with network in a wind energy conversion system. In: TerraGreen 13 International Conference 2013 on Advancements in Renewable Energy and Clean Environment; 15–17 February 2013; Beirut, Lebanon. Amsterdam, the Netherlands: Energy Procedia. pp. 169-178.

[22] Haque MH. Damping improvement by FACTS devices: a comparison between STATCOM and SSSC. Electr Pow Syst Res 2006; 76: 865-872.

[23] Zhang XP, Handschin E, Yao M. Multi-control functional static synchronous compensator (STATCOM) in power system steady-state operations. Electr Pow Syst Res 2004; 72: 269-278.

[24] Ezoji H, Sheikholeslami A, Rezanezhad M, Livani H. A new control method for dynamic voltage restorer with asymmetrical inverter legs based on fuzzy logic controller. Simul Model Pract Th 2010; 18: 806-819.

Appendix. WECS parameters.

$$G = 45; R = 8\,m;\ f = 0.0024\,Nm\frac{s}{rd};\ J = 100\,Kgm^2;\ L_s = 0.01545\,H;$$

$$L_r = 0.25454\,H;\ M = 0.0151\,H; p = 2\,;P_n = 75\,kW;\ R_r = 0.02092\,\Omega;$$

$$R_s = 0.03552\,\Omega; U_n = 400\,V$$